Surface and confined optical phonons in CdS$_x$Se$_{1-x}$ nanoparticles in a glass matrix

Anushree Roy

Department of Physics, Indian Institute of Science, Bangalore 560 012, India

Ajay K. Sood

Department of Physics, Indian Institute of Science, Bangalore 560 012, India
and Jawaharlal Nehru Center for Advanced Scientific Research, Jakkur Campus, P.O. Jakkur, Bangalore 560 064, India

We report first- and higher-order Raman scattering from the surface and confined optic phonons in CdS$_{0.65}$Se$_{0.35}$ and pure CdS nanoparticles embedded in glass matrix. The average particle sizes and size distribution have been estimated from the quantitative comparison of the blue-shifted optical-absorption spectra with the calculations based on the tight-binding model. The first-order asymmetric Raman line shape has been analyzed by including both the confined optic modes and the surface modes. The average particle sizes so obtained from this analysis compare well with those estimated from the optical-absorption spectra. The observed frequencies of the surface modes have been compared with the results of the dielectric response function model.

I. INTRODUCTION

In recent times optical properties of semiconductor nanocrystals have attracted considerable attention as they differ significantly from those of the corresponding bulk crystals. In a bulk crystal, the phonon eigenstate is a plane wave and the wave vector selection rule for first-order Raman scattering requires $q \simeq 0$. In contrast, the spatial correlation function of the phonon becomes finite due to its confinement in the microcrystals and hence the $q \simeq 0$ rule is relaxed. In general, since the phonon-dispersion curves of bulk crystal show the frequency ω to be a decreasing function of wave vector $|\vec{q}|$, the first-order Raman line redshifts and broadens with asymmetry towards the low-frequency side as observed for Si and BN microcrystals.[1,2] This has been explained in a phenomenological phonon confinement model proposed by Richter *et al.*[1] This model assumes that the bulk phonon-dispersion curves are not affected and no new modes are created due to the size reduction of the crystal. Many other studies have shown the presence of confined optic phonons in microcrystallites.[3–5]

For a plane wave propagating in the x direction in a bulk crystal, the temporal and spatial variation of the wave is described by the factor $\exp[i(kx-\omega t)]$, where the wave vector $k = (\omega/c)\sqrt{\epsilon(\omega)}$; $\epsilon(\omega)$ is the dielectric constant of the crystal. In the frequency range between bulk longitudinal-optical (LO) phonon frequency, $\omega(\text{LO})$ and transverse-optical (TO) phonon frequency $\omega(\text{TO})$, $\epsilon(\omega) < 0$ making k imaginary and hence the wave decays exponentially in the medium. Therefore in this frequency range, electromagnetic wave cannot propagate in bulk crystal and only the surface modes with spatially decaying fields (away from the surface) satisfying the boundary conditions exist. These surface modes can be observed more easily in nanoparticles because of their enhanced surface to volume ratio. Let us consider a sphere of radius R and dielectric constant $\epsilon(\omega)$, embedded in a medium with dielectric constant ϵ_m. Following Fuchs and Kliewer,[6] the electric potential and normal component of the displacement vector are matched across the particle-matrix interface to give an equation to calculate the frequencies of the surface phonons: $\epsilon(\omega) = -(l+1)\epsilon_m/l$ where $l = 1, 2, \ldots$. The mode with $l = 1$, called the Frölich mode, is uniformly polarized with eigenfrequency given by $\epsilon(\omega_F) = -2\epsilon_m$. It is a dipolar mode and corresponds to the uniform polarization of the sphere. The field becomes more localized for modes $l \geqslant 2$. The $l = 2$ is a quadrupole mode and the first of the surface mode series.

Infrared reflectivity measurements of microcrystallites of UO$_2$ and ThO$_2$, supplemented with static dc and near-infrared-absorption measurements have shown the presence of surface modes.[7,8] Ruppin and Englman have discussed the possibility of observing surface phonons by light scattering in small crystallites of spherical, cylindrical or slablike geometries.[9] Scott and Damen observed surface phonons in small ($\ll 1$ μm) crystallites of CdS in a polycrystalline film using Raman scattering.[10] The Raman spectra of GaP microcrystals have been decomposed into TO, LO, and surface phonon (SP) peaks.[11] These measurements show that the ratio of the integrated intensities $I_{\text{sp}}/I_{\text{TO}}$ depends on the particle size. The asymmetric lineshape of the SP peak attributed to ellipsoidal shape of the particles was calculated based on the effective-medium theory.[11] Klein *et al.* studied the size dependence of the Fröhlich electron-phonon coupling for semiconductor nanospheres.[12] They derived the expressions of the relevant eigenfunctions corresponding to longitudinal optic and surface modes and showed that the coupling strength is independent of the size of the nanoparticles, provided the typical dimensions of the electronic charge distribution scale as the sphere radius. The experimental results obtained using resonant Raman scattering from CdSe-doped glasses with particles of various sizes qualitatively confirm the size independence of the coupling strength and also show the presence of the surface modes.[12] Optical surface phonons have also been observed by Zhou *et al.* using Raman spectroscopy of CdS$_x$Se$_{1-x}$ nanoparticles doped in the glass medium.[13] They show that the intensity of the SP peak increases but its position remains unchanged as the size of the

nanoparticles decreases, in agreement with the earlier work.[9] The SP frequency changes as a function of alloy content in $(CdS)_x(CdSe)_{1-x}$ nanoparticles.[14]

In this paper we report our Raman studies of the confined optical modes and surface modes in (i) commercial Schott filter glass OG590, which has $CdS_{0.65}Se_{0.35}$ particles embedded in borosilicate glass matrix and (ii) CdS particles embedded in silica matrix. We have estimated the average size and the size distribution of the particles in these samples by matching the measured blue-shifted absorption spectra and the calculated optical-absorption spectra. The calculations take into account the log-normal distribution of particle diameters in conjunction with the allowed electronic transition states as obtained from the effective tight-binding model.[15] Unlike the previous reports,[9,12–14] the asymmetric Raman line shape has been quantitatively analyzed by including both the confined optic modes and the surface modes. The observed frequencies of the SP modes in these systems have been compared with the calculations based on the dielectric response function model.

II. EXPERIMENTAL

Experiments have been carried out on commercially available Schott filter glass OG590 which has $CdS_{0.65}Se_{0.35}$ nanoparticles and CdS particles in silica matrix. The latter have been prepared by us using the sol-gel route.[16] In this preparation, tetraethoxysilane (TEOS), $Si(OC_2H_5)$, is partially hydrolyzed by adding it into a mixed solution of H_2O, C_2H_5OH, and HCl. The molar ratio of TEOS:water:alcohol:acid is kept at 1:4:11:0.03. After the solution is stirred for 1 h, $Cd(NO_3)_2$ dissolved in 1 mole of water is added followed by stirring the solution for 1 h at room temperature. The molar ratio of the $Cd(NO_3)_2$ is varied from 0.0077 to 0.195 mol per 1 mol of TEOS. The sol is poured into a petri dish and allowed to evaporate at room temperature till it becomes a solid gel. This gel is heated at 250 °C for 1 h. The CdS particles are formed by flowing dry H_2S gas through the gel for 1 h at room temperature. The size of the CdS particles is controlled by the amount of $Cd(NO_3)_2$ added to the solution. For the present studies we have prepared the sample by adding 0.05 mol of $Cd(NO_3)_2$ in 1 mol of TEOS. Optical-absorption spectra were recorded for 1-mm-thick optically polished samples using UV-visible spectrometers Hitachi model 150-20 and Pye-Unicam model SP8-100. Raman spectra were recorded at room temperature in the backscattering geometry for the CdS particles in silica matrix and in 90° geometry for the OG590 sample using a 5145 Å line of argon ion laser as excitation source (power ~ 20 mW) and computer controlled SPEX Ramalog (model 14018) with cooled photomultiplier tube and photon counting electronics.

III. RESULTS AND DISCUSSION

A. $CdS_{0.65}Se_{0.35}$ particles in glass matrix (OG590)

1. Optical absorption

Figure 1 shows the optical-absorption spectrum of OG590. The band gap of bulk $CdS_{0.65}Se_{0.35}$ is 2.05 eV (605 nm).[17] For the microcrystallites the first absorption band appears at ~ 552 nm (2.26 eV). The blueshift in the optical-
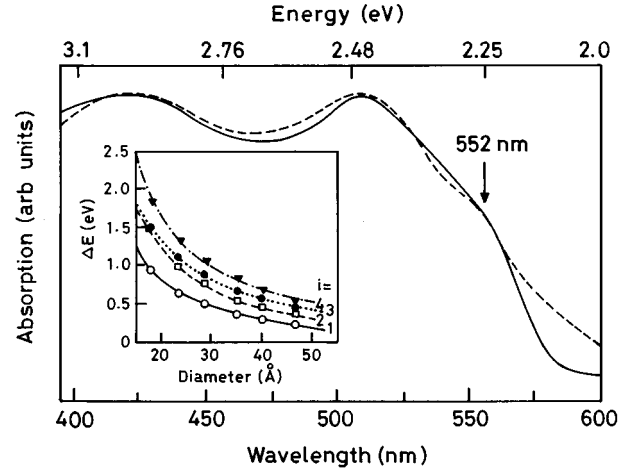
FIG. 1. Measured (solid line) and calculated (dotted line) absorption spectra of the sample OG590. The arrow marks the band-gap of the $CdS_{0.65}Se_{0.35}$ microcrystallites. Inset: The points show the variation of ΔE with respect to particle diameter d for different transitions in the tight-binding model. The curves through the points are fit to $\Delta E = A_i/d^{x_i}$.

absorption spectra arises from the confinement of the charge carriers in the microcrystallites. The optical-absorption coefficient of a collection of monodispersed microcrystallites of diameter d at low temperature is given by

$$\alpha(E) \sim \sum_i \frac{f_i \Gamma_i}{(E - E_i)^2 + \Gamma_i^2}, \qquad (1)$$

where f_i is the oscillator strength, E_i is the transition frequency, and Γ_i is the half width at half maximum (HWHM) for the ith interband transition. The sum is over all the transitions from filled levels to the unfilled ones. This should result in sharp optical-absorption peaks as already observed in CuCl microcrystals dispersed in a transparent insulating matrix.[18] However, the absorption spectrum in Fig. 1 does not show sharp absorption peaks. This is due to thermal broadening as well as inhomogeneous broadening due to particle size distribution. The latter can be included in Eq. (1) to give

$$\alpha_{\text{observed}}(E) = B \sum_i \int_0^\infty d(d) \frac{P(d) f_i \Gamma_i}{[E - E_i(d)]^2 + \Gamma_i^2}, \qquad (2)$$

where $P(d)$ is the size distribution usually taken to be log-normal, as

$$P(d) = \frac{1}{d\sigma\sqrt{2\pi}} \exp\left(-\frac{\ln^2(d/\bar{d})}{2\sigma^2}\right). \qquad (3)$$

Here $\bar{d}$ and σ are related to the average size and the size distribution of the particles. The average size (d_{av}) of the particles has been estimated numerically by

$$d_{\text{av}} = \int_0^\infty d \cdot P(d) d(d) \qquad (4)$$

for a given $\bar{d}$ and σ.

TABLE I. The variation of the electronic transition frequency with the particle size follows the relation $\Delta E = A_i/d^{x_i}$. ΔE is expressed in eV and d in Å.

i	Electronic transitions	A_i	x_i	f_i	Γ_i (meV)
1	$1\Gamma_8^- \text{-} 1\Gamma_6^+$	84.5	1.54	4.13	30
	$1\Gamma_7^- \text{-} 1\Gamma_6^+$	84.5	1.54	1.73	30
	$1\Gamma_8^+ \text{-} 1\Gamma_7^-$	112.4	1.49	1.48	50
2	$1\Gamma_8^+ \text{-} 1\Gamma_8^-$	112.4	1.49	2.28	50
	$1\Gamma_6^+ \text{-} 1\Gamma_7^-$	112.4	1.49	1.41	50
	$1\Gamma_6^+ \text{-} 1\Gamma_8^-$	112.4	1.49	0.69	50
3	$\Gamma_8^+ \text{-} 1\Gamma_8^-$	64.6	1.30	1.53	65
	$2\Gamma_8^+ \text{-} 1\Gamma_7^-$	64.6	1.30	0.32	65
4	$2\Gamma_7^+ \text{-} 1\Gamma_8^-$	78.8	1.29	1.12	80
	$3\Gamma_8^+ \text{-} 1\Gamma_7^-$	78.8	1.29	0.56	80
	$3\Gamma_8^+ \text{-} 1\Gamma_8^-$	78.8	1.29	0.23	80

FIG. 2. Dots show the measured first-order Raman spectrum of the sample OG590 using a 5145 Å line as an excitation source. The solid line is a fit to $I_c(\omega)+I_{sp}(\omega)$. The dashed lines show the contributions of the individual components $I_c(\omega)$ and $I_{sp}(\omega)$. The inset shows the CdS-like mode with the fit (dotted line) only with $I_c(\omega)$.

The interband transition energy is given by $E^{trans}= E_g^{bulk} + E_{conf} + E_{coul}$ where E_g^{bulk} is the band gap of the bulk semiconductor, E_{conf} is the electron-hole pair confinement kinetic energy, and E_{coul} is the Coulomb interaction energy between the electron and the hole. The simplest interpretation of the optical-obsorption spectra is in terms of single-band effective-mass approximation (EMA). The Coulomb interaction between the electron and hole estimated in first-order perturbation theory using single band EMA wave functions is given by $E_{coul}=-1.786\, e^2/\epsilon R$, where ϵ is the dielectric constant of the material and R is the radius of the microcrystallite.[19,20] In EMA the confinement kinetic energy corresponding to the lowest energy transition is $E_{conf}= h^2\pi^2/2\mu R^2$ where μ is the reduced effective mass, $\mu^{-1}= m_e^{\star -1} + m_h^{\star -1}$, $m_e^{\star}$ and $m_h^{\star}$ are the effective masses of the electron and hole respectively.[21] The results of single band EMA do not agree with the optical-obsorption spectra of microcrystallites because it neglects intervalence band mixing and deviation from quadratic dispersion. The band mixing included within EMA by multiband calculations do not result in good agreement with the experiments, especially in smaller size microcrystallites. It has been shown[15] that the tight-binding calculations yield energy levels in close agreement with the experiments. Here we shall rely upon the results of Ramaniah and Nair [15] based on tight-binding calculations of the interband optical transitions in quantum dots. The following interband transitions are considered: $1\Gamma_8^- \text{-} 1\Gamma_6^+$, $1\Gamma_7^- \text{-} 1\Gamma_6^+$, $1\Gamma_8^+ \text{-} 1\Gamma_7^-$, $1\Gamma_8^+ \text{-} 1\Gamma_8^-$, $1\Gamma_6^+ \text{-} 1\Gamma_7^-$, $1\Gamma_6^+ \text{-} 1\Gamma_8^-$, $2\Gamma_8^+ \text{-} 1\Gamma_8^-$, $2\Gamma_8^+ \text{-} 1\Gamma_7^-$, $2\Gamma_7^+ \text{-} 1\Gamma_8^-$, $3\Gamma_8^+ \text{-} 1\Gamma_7^-$, $3\Gamma_8^+ \text{-} 1\Gamma_8^-$. These are grouped in four types ($i = 1$ to 4) as given in Table I. The calculated values of[15] $\Delta E = E_i - E_g^{bulk} = E_{conf} + E_{coul}$ for these transitions, are plotted as a function of microcrystallite diameter in the inset of Fig. 1. In order to get an analytic form of $E_i(d)$ required in Eq. (2), we find that the particle size dependence of ΔE is much milder than $1/d^2$. This guided us[22] to assume an empirical relation $\Delta E = A_i/d^{x_i}$ where A_i and x_i are constants for a particular transition obtained from fitting the calculated values. The lines in the inset show these fits with parameters A_i and x_i listed in

Table I. Here ΔE is expressed in eV and d in Å. Since the oscillator strength is not very sensitive to particle diameter for $\bar{d} \geq 30$ Å,[15] the value of f_i listed in Table I corresponds to those of $d = 46$ Å. Taking, $E_i(d)=E_g^{bulk}+A_i/d^{x_i}$, $\sigma=0.12\pm0.02$ and $\bar{d} = 98$ Å ± 3 Å, the calculated optical-absorption spectrum [Eqs. (2) and (3)] is shown by dashed line in Fig. 1. It can be seen that the agreement between the calculated and experimental spectra is reasonably good except at higher wavelengths. For these values of σ and $\bar{d}$ the average size of the particle is the same as $\bar{d}$ and full width at half maximum (FWHM) of $P(d)$ is 18 Å.

2. First-order Raman scattering: confined optical phonons and surface phonons

First-order Raman spectrum of the sample $CdS_{0.65}Se_{0.35}$ shows two-mode behavior [Fig. 2]. As can be seen, each of these modes shows an asymmetric line shape towards the lower-frequency side. Using phonon confinement model and following Campbell and Fauchet,[23,24] the first-order Raman spectrum $I_c(\omega)$ is given by

$$I_c^j(\omega)=A^j \int^{q_{max}} \frac{d\vec{q}\,|C(0,\vec{q})|^2}{[\omega-\omega^j(\vec{q})]^2+(\Gamma_c)^2}, \qquad (5)$$

where $\omega^j(\vec{q})$ is the phonon-dispersion function of the corresponding bulk material and $C(0,\vec{q})$ is the Fourier coefficient of the phonon confinement function $W(r,d)$. Γ_c is the HWHM of the phonon line in the bulk crystal. The superscript $j = 1$ is for CdS-like and $j =2$ is for CdSe-like modes. The confinement function is taken to be $W(r,d)$
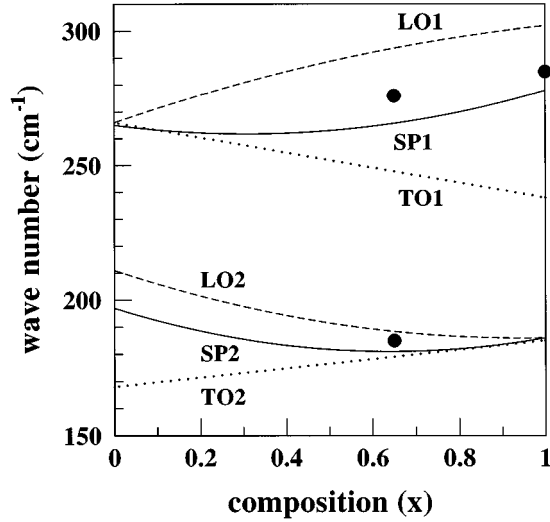
FIG. 3. Solid lines show the x dependence of the calculated surface phonon frequencies based on Eq. (10). The dashed and dotted lines show the x dependence of the bulk LO and TO phonon frequencies, respectively. The dots are the measured value of the SP for the two samples studied.

$=\exp(-8\pi^2 r^2/d_{av}^2)$, so that $|C(0,\vec{q})|^2 = \exp(-q^2 d_{av}^2/4a^2)$; here d_{av} is the average diameter of the spherical microcrystal.[23] This form of confinement function has been shown to work better than the Lorentzian or the exponential functions.[23] The wave vector $\vec{q}$ has been expressed in units of $2\pi/a$ (where a is the lattice constant $= 6.8$ Å). The average phonon dispersion for the j mode in the bulk CdS $_x$Se$_{1-x}$ crystal for the LO phonon is taken[25] to be

$$\omega^j(q) = \omega_0^j - \Delta\omega^j \sin^2(q/4),$$

which fits the experimental curve well in the direction Γ-M up to $q_{max} = 0.6$. ω_0^j is the corresponding bulk LO phonon frequency: $\omega_0^1 = 292$ cm^{-1} and $\omega_0^2 = 199$ cm^{-1}. The band width ($\Delta\omega^j$) of the LO branch for both the CdS-like and CdSe-like mode are taken to be 30 cm^{-1} (Ref. 25) and Γ_c as estimated from the Raman spectrum of the bulk crystal is taken as 4 cm^{-1} (this also includes in a simple way the effect of finite instrumental resolution). Following Eq. (5), we tried to fit the experimental Raman spectrum of OG590 using this model alone, where the best fit obtained for the CdS-like mode is shown by dashed line in the inset of Fig. 2 and the corresponding value of chisquare (χ^2) is 0.31. It is obvious from the above figure and the low value of χ^2 that phonon confinement model alone cannot fully explain the observed Raman line shape. Keeping in mind the possibility of the presence of the SP together with the confined optical phonon, we have attempted to fit the observed line shape

TABLE II. CdS and CdSe parameters used in the calculation.

	ω_{LO}(Ref. 3)(cm^{-1})	ω_{TO}(Ref. 3)(cm^{-1})	ϵ_∞(Ref. 3)
CdS	$266+55x-19x^2$	$266-28x$	5.32
CdSe	$211+53x-28x^2$	$168+17x$	6.1
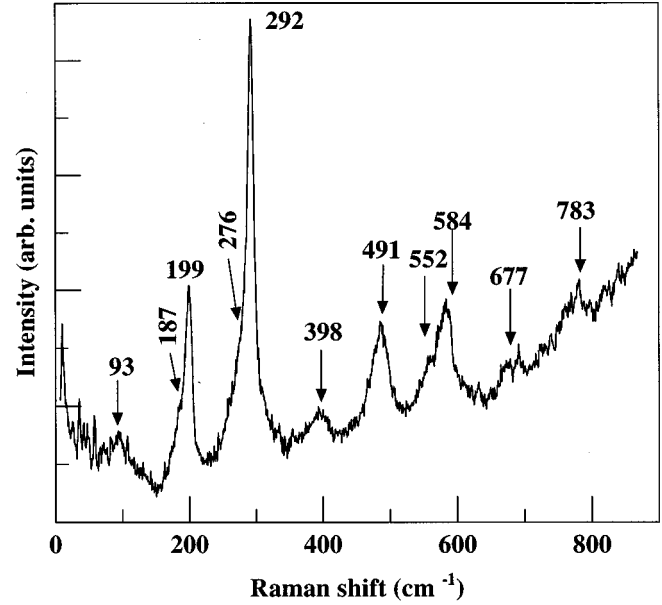
FIG. 4. Raman spectrum of OG590 showing higher-order Raman scattering.

with a combined line shape $I^j(\omega) = I_c^j(\omega) + I_{sp}^j(\omega)$, where $I_{sp}^j(\omega)$ is taken to be a Lorentzian function

$$I_{sp}^j(\omega) = \frac{B^j \Gamma_{sp}^j}{(\omega - \omega_{sp}^j)^2 + (\Gamma_{sp}^j)^2} \qquad (6)$$

Γ_{sp}^j is the HWHM for the jth SP mode. The best fit obtained is shown by the solid line in Fig. 2 and the corresponding value of χ^2 is 0.83, much closer to the ideal value of 1. The confined optic phonon and the surface phonon components are shown by the dashed line in Fig. 2. The average particle size (d_{av}) obtained from the nonlinear least-squares fit is 95 ± 2 Å, which is very close to the average size of the particles obtained for the analysis of the optical-absorption spectrum. The fit gives the SP frequencies to be 276 and 187 cm^{-1}.
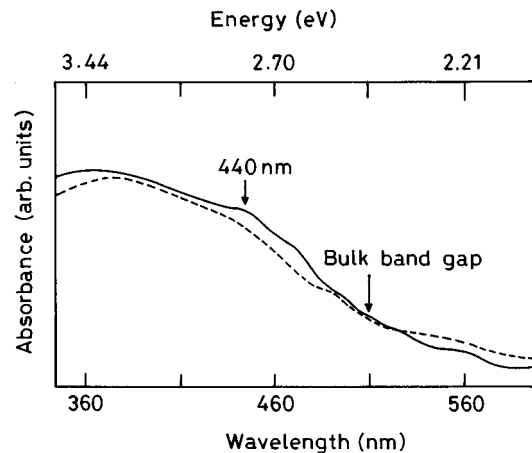
FIG. 5. Measured (solid line) and calculated (dotted line) optical-absorption spectra of CdS particles in the silica matrix.

It is known that in binary alloys, the behavior of the optical modes can be accounted for by considering two types of oscillators interacting via their electric fields. The effective oscillator strength is proportional to the density of the oscillators. Assuming nonoverlapping restrahlen bands for these two modes, $\omega_{LO1} > \omega_{TO1} > \omega_{LO2} > \omega_{TO2}$, the dielectric response function of a mixed crystal can be written as

$$\epsilon(\omega) = x\epsilon_1(\omega) + (1-x)\epsilon_2(\omega), \qquad (7)$$

with $\epsilon_1(\omega)$ and $\epsilon_2(\omega)$ are given by

$$\epsilon^j(\omega) = \epsilon_\infty^j \left[1 + \frac{\omega_{LOj}^2 - \omega_{TOj}^2}{\omega_{TOj}^2 - \omega^2} \right], \qquad (8)$$

where ϵ_∞ is the high-frequency dielectric constant of the crystal. Substituting Eq. (8) in Eq. (7) for both the CdSe and CdS like modes and using $\epsilon(\omega) = -(l+1)\epsilon_m/l$ we get the following equation for the surface phonon frequencies of the binary mixed crystal:

$$\omega^4 - \omega^2 \left[\omega_{TO1}^2 + \omega_{TO2}^2 + \frac{x\epsilon_\infty^1}{K}(\omega_{LO1}^2 - \omega_{TO1}^2) \right.$$
$$\left. + \frac{(1-x)\epsilon_\infty^2}{K}(\omega_{LO2}^2 - \omega_{TO2}^2) \right]$$
$$+ \omega_{TO1}^2 \omega_{TO2}^2 \left[1 + \frac{x\epsilon_\infty^1}{K} \frac{(\omega_{LO1}^2 - \omega_{TO1}^2)}{\omega_{TO1}^2} \right.$$
$$\left. + \frac{(1-x)\epsilon_\infty^2}{K} \frac{(\omega_{LO2}^2 - \omega_{TO2}^2)}{\omega_{TO2}^2} \right] = 0, \qquad (9)$$

where $K = (l+1)\epsilon_m/l + x\epsilon_\infty^1 + (1-x)\epsilon_\infty^2$. Here ω_{LOj} and ω_{TOj} are the x-dependent values of the longitudinal and transverse modes for CdS ($j=1$) and CdSe ($j=2$) crystals. Note that Eq. (9) gives the surface phonon frequencies of a mixed crystal which are assumed to be the same for the bulk and the microcrystallite. Using Eq. (9), the solid lines in Fig. 3 show the variation of CdS-like and CdSe-like SP frequencies with x for $l=2$. The bulk LO and TO phonon frequencies for the different values of x used in Eq. (9) are shown by dashed and dotted lines, respectively, for both the modes. The parameters used for the calculations are summarized in Table II. The values of other parameters are $\epsilon_m = 2.25$, $\epsilon_\infty^1 = 6.1$ and $\epsilon_\infty^2 = 5.32$. The calculated SP frequencies ω_{sp} in pure CdS is 281 cm^{-1} ($l=2$). These frequencies for $l=2$ in OG590 ($x=0.65$) are $\omega_{sp}^1 = 266$ cm^{-1} and $\omega_{sp}^2 = 183$ cm^{-1}, which can be compared well with the observed $\omega_{sp}^1 = 276$ cm^{-1} and $\omega_{sp}^2 = 187$ cm^{-1}. The values of Γ_{sp}^j are 12.3 cm^{-1} ($j=1$) and 10 cm^{-1} ($j=2$). The ratios of A/B are 2×10^4 and 1.2×10^4 for CdS-like and CdSe-like mode. The filled circles in Fig. 3 represent the measured SP frequencies for pure CdS ($x=1$) and for OG590 ($x=0.65$). Here it should be noted that similar calculation has been reported by Mlayah et al.[14] but their expression for ω_{sp}^2 does not give the correct results in the limits of $x=0$ and 1.

Under resonance conditions, multiphonon Raman scattering can also be observed. Figure 4 shows multiphonon Raman spectrum of the sample OG590 using 5145 Å line of
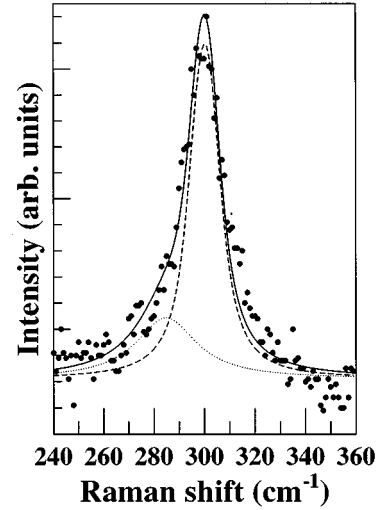
FIG. 6. First-order Raman spectrum of CdS particles in silica matrix.

argon-ion laser as the excitation source. In addition to the first-order Raman line for CdS-like mode [LO(1)] at 292 cm^{-1} and CdSe-like mode [LO(2)] at 199 cm^{-1}, the higher-order spectrum is observed showing a difference mode LO(1)−LO(2) at 93 cm^{-1}, overtones 2LO(1) at 584 cm^{-1}, 2LO(2) at 398 cm^{-1}, combination mode LO(1)+LO(2) at 491 cm^{-1} and 2LO(1)+LO(2) at 783 cm^{-1}. The mode at 677 cm^{-1} can perhaps be 3LO(1)−LO(2) or 2LO(2)+SP(1) and the mode at 552 cm^{-1} can be 2SP(1), corroborating the value of $\omega_{SP}^1 = 276$ cm^{-1} as deduced from the earlier analysis of the first-order Raman spectra.

B. CdS particles in glass matrix

The optical-absorption spectrum of the CdS particles embedded in silica matrix is shown in Fig. 5. The bulk band gap of pure CdS is 2.38 eV (521 nm).[17] For the microcrystallites the absorption band appears at $\sim$ 2.82 eV (440 nm). Following the same procedure as we have used for the sample OG590, the calculated optical-absorption spectrum with $\sigma = 0.5$ and $\bar{d} = 40 \pm 3$ Å is shown by dashed line in Fig. 5. For these values of σ and $\bar{d}$ the average size of the particles is 45 ± 3 Å and FWHM is rather large $\sim$ 40 Å.

The first-order Raman spectrum shows an asymmetric Raman line (Fig. 6) which can be explained as before using $I(\omega) = I_c(\omega) + I_{sp}(\omega)$ [Eqs. (5) and (6)]. The best fit obtained is shown by the solid line in Fig. 6. The SP component and optical-phonon component are shown by dotted line and dashed line, respectively. The fit yields the average particle size to be 48 Å and the SP frequency $\omega_{sp} = 285$ cm^{-1}. The latter compares well with the calculated ω_{sp} ($l=2$) of 281 cm^{-1}.

IV. CONCLUSIONS

We have shown that the first-order Raman line of nanoparticles can be quantitatively explained by taking into ac-

count the confined optical-phonon modes and the SP modes. The average size of the particles obtained from the fit of the Raman line shape agree very well with those obtained from the analysis of the optical-absorption spectra with inputs from the tight-binding model for the transition frequencies. The observed surface phonon frequencies have been compared with the calculated ones using dielectric response func-

tion model. We have also reported the multiphonon Raman scattering in the sample OG590.

[1] H. Richter, Z.P. Wang, and L. Ley, Solid State Commun. **39**, 625 (1981).

[2] R.J. Nemanich, S.A. Solin, and R.M. Martin, Phys. Rev. B **23**, 6348 (1981).

[3] R. Tsu, H. Shen, and M. Dutta, Appl. Phys. Lett. **60**, 112 (1992).

[4] A.K. Sood, K. Jayaram, and D.V.S. Muthu, J. Appl. Phys. **72**, 4963 (1992).

[5] A. Roy, K. Jayaram, and A.K. Sood, Solid State Commun. **89**, 229 (1994).

[6] R. Fuchs and K.L. Kliewer, J. Opt. Soc. Am. **58**, 319 (1968).

[7] J.D. Axe and G.D. Pellit, Phys. Rev. **151**, 676 (1966).

[8] W.W. Pultz and W. Hertl, Spectrochim. Acta **22**, 573 (1966).

[9] R. Ruppin and R. Englman, Rep. Prog. Phys. **33**, 149 (1970).

[10] J.F. Scott and T.C. Damen, Opt. Commun. **5**, 410 (1972).

[11] S. Hayashi and R. Ruppin, J. Phys. C **18**, 2583 (1985).

[12] M. C. Klein, F. Hache, D. Ricard, and C. F. Flytzanis, Phys. Rev. B **42**, 11 123 (1990).

[13] F. Zhou, Y. Sun, and J. Pan, J. Lumin. **40 & 41**, 739 (1988).

[14] A. Mlayah, A.M. Brugman, R. Caries, J.B. Renucci, M. Ya. Valakh, and A.V. Pogerolov, Solid State Commun. **90**, 567 (1994).

[15] L.M. Ramaniah and S.V. Nair, Phys. Rev. B **47**, 7132 (1993).

[16] M. Nogami, K. Nagasaka, and M. Takata, J. Non-Cryst. Solids **122**, 101 (1990).

[17] M. Hayek and O. Brafman, in *Light Scattering in Solids*, edited by M. Balkanski (Flammirion, Paris, 1971), p. 76.

[18] A.I. Ekimov and A.A. Onushchenko, Sov. Phys. Semicond. **16**, 775 (1982).

[19] L. E. Brus, J. Chem. Phys. **80**, 4403 (1984).

[20] L. E. Brus, J. Chem. Phys. **79**, 5566 (1983).

[21] AI. L. Efros and A. L. Efros, Sov. Phys. Semicond. **16**, 772 (1982).

[22] A. Roy and A.K. Sood, Solid State Commun. **97**, 97 (1995).

[23] H. Campbell and P. M. Fauchet, Solid State Commun. **58**, 739 (1986).

[24] P. M. Fauchet and I. H. Campbell, Crit. Rev. Solid State Mater. Sci. **14**, S79 (1988) and the references therein.

[25] H. Bilz and W. Kress, *Phonon Dispersion Relations in Insulators* (Springer-Verlag, Berlin, 1979), p. 120.